scientific reports

Check for updates

OPEN

Theoretical studies on donor–acceptor based macrocycles for organic solar cell applications

Sheik Haseena & Mahesh Kumar Ravva✉

We have designed a series of new conjugated donor–acceptor-based macrocyclic molecules using state-of-the-art computational methods. An alternating array of donors and acceptor moieties in these macrocycle molecules are considered to tune the electronic and optical properties. The geometrical, electronic, and optical properties of newly designed macrocyclic molecules are fully explored using various DFT methods. Five conjugated macrocycles of different sizes are designed considering various donor and acceptor units. The selected donor and acceptors, viz., thiophene (PT), benzodithiophene (BDT), dithienobenzodithiophene (DTBDT), diketopyrrolopyrrole (DPP), and benzothiazole (BT), are frequently found in high performing conjugated polymer for different organic electronic applications. To fully assess the potential of these designed macrocyclic derivatives, analyses of frontier molecular orbital energies, excited state energies, energy difference between singlet–triplet states, exciton binding energies, rate constants related to charge transfer at the donor–acceptor interfaces, and electron mobilities have been carried out. We found significant structural and electronic properties changes between cyclic compounds and their linear counterparts. Overall, the cyclic conjugated D–A macrocycles' promising electronic and optical properties suggest that these molecules can be used to replace linear polymer molecules with cyclic conjugated oligomers.

Macrocyclic π-conjugated molecules have recently emerged as a new family of materials due to their unique structural and electronic properties[1–5]. Macrocyclic π-conjugated molecules have several advantages: controlled structure, delocalized π-space, well-defined cavity to host electronically active materials, better intermolecular arrangement, three-dimensional charge transport, and lower aggregation[6,7]. The design and development of new cyclic π-conjugated compounds, such as cyclothiophenes, cyclo-para-phenylenes (CPP), and cyclo-meta-phenylenes, have opened up new avenues for research in macrocyclic compounds[2,8,9]. Numerous reports demonstrated the applications of these materials in organic solar cells (OSCs), organic field-effect transistors (OFETs), organic light-emitting diodes (OLEDs), sensors, and photodetectors[10–14]. The choice of donor/acceptor building units and linkers dictates macrocycles' electronic and optical properties similar to conventional conjugated donor–acceptor polymers. Effective synthetic chemistry strategies have been utilized to synthesize various types of macrocycles, which are composed of triphenylamine, carbazole, thiophene, furan, acetylene, perylenediimides, etc[4,6,15,16].

Non-fullerene acceptors with acceptor–donor–acceptor (A–D–A) units are efficient topologies for tuning HOMO–LUMO energy levels, altering the band gap, and improving absorption strength. The above-mentioned building blocks have exceptionally enhanced the performance of OSCs power conversion efficiency (PCE) of 18%)[17–21]. PCE determines how much incident light is converted to electrical energy. It is measured as the ratio of electrical output to incident solar power and expressed as PCE = (J*sc* x V*oc* x FF)/P_{in}, where J*sc* denotes short circuit current, V*oc* stands for open circuit voltage, FF stands for fill factor, and P_{in} represents the power of an incident ray of light.

Thus, the design and development of novel NFA molecules have huge application potential. Particularly, the investigations on the NFA molecules comprising donor–acceptor-based π-conjugated macrocyclic molecules have paramount importance in the development of the new class of materials[22,23]. Li et al. have synthesized diketopyrrolopyrrole (DPP) based donor–acceptor macrocyclic conjugated molecules, and these materials were used as electron acceptors in OSCs. Various attributes of these macrocyclic molecules include (i) the three-dimensional

Department of Chemistry, SRM University-AP, Guntur, Andhra Pradesh 522240, India. ✉email: mahesh.r@srmap.edu.in

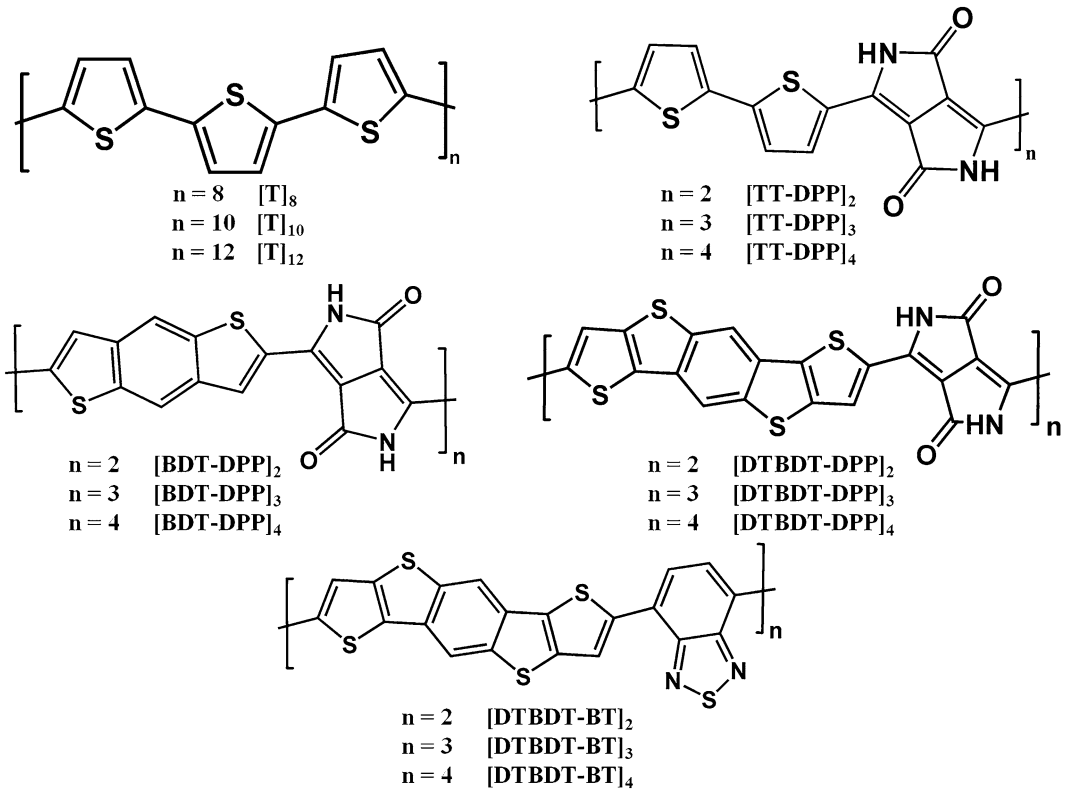

Figure 1. Chemical structures of donor–acceptor based conjugated systems considered in this study.

shape, (ii) conjugated π-electronic delocalization, and (iii) low-energy unoccupied molecular orbital (LUMO), rendering these macrocycles as pseudo fullerenes[6]. The experimental studies of cyclo-phenylene-thienylenes (CPT) showed that the LUMO energy decreases with the increase of ring size. However, there was no substantial change in the HOMO energy[4]. At the same time, red-shift in absorption maxima and considerable blue shift in fluorescence maxima in CPT have been noticed. Similarly, Zhang et al. reported triphenylamine and benzothiadiazole-based donor–acceptor conjugated macrocycle[2]. Further, these authors have fabricated solar cells using C_{60} derivatives as acceptor units. Both scanning tunneling microscopy (STM) and density functional theory (DFT) based calculations have been employed to understand the morphology and electronic structure. A host–guest architecture of fullerene acceptors encapsulated inside cycloparaphenylene (CPP) and its derivatives have also been reported. It is found that the solid-state packing directly impacts morphology and charge transfer. The predicted PCE using microscopic charge transport parameters and a time-domain drift–diffusion model is found to be 9%[24].

In view of the significance of macrocyclic π-conjugated materials, we have designed and developed macrocyclic compounds employing electronic structure theory. Since thiophene-based molecules have received widespread attention from researchers in the development of materials for organic electronic materials, polythiophenes-based macrocyclic π-conjugated compounds have been considered. Furthermore, the thiophene unit has been systematically replaced with different donor and acceptor units to develop various new conjugated donor–acceptor macrocycles. Density functional theory methods are used to evaluate the electronic and optical properties, viz., energy levels, absorption spectra, and charge transport properties. Appropriate combinations of donor and acceptor units have been optimized by considering geometrical and electronic factors. In this context, we have taken into consideration of various critical parameters such as variation of molecule size, shape, length, orientation, and self-assembling nature, which in turn influence the nature of π-conjugation. In addition, corresponding linear counterparts have been studied to compare changes in the electronic and optical properties upon cyclization. Attempts have been made to compare experimental findings wherever possible. Overall, the findings from this study would pave the way for the development of a novel class of compounds for organic solar cell applications. The schematic representation of models considered in this study is shown in Fig. 1. As described earlier, in order to understand the impact of the size of the macrocycle on the electronic and optical properties, three different ring sizes are considered. Cyclic and linear oligothiophenes with 8, 10, and 12 repetitive thiophene units ($C[PT]_n$ and $L[PT]_n$, where n = 8, 10, and 12, respectively) were considered[25]. As shown in Fig. 1, four donor–acceptor-based macrocycles ($C[TT\text{-}DPP]_n$, $C[BDT\text{-}DPP]_n$, $C[DTBDT\text{-}DPP]_n$, and $C[DTBDT\text{-}BT]_n$) are designed by considering three donor units such as bithiophene (TT), benzodithiophene (BDT), dithienobenzodithiophene (DTBDT); and two acceptor units such as diketopyrrolopyrrole (DPP), and benzothiazole (BT)[6,26–31]. In order to understand the impact of cyclization, linear counterparts are also considered

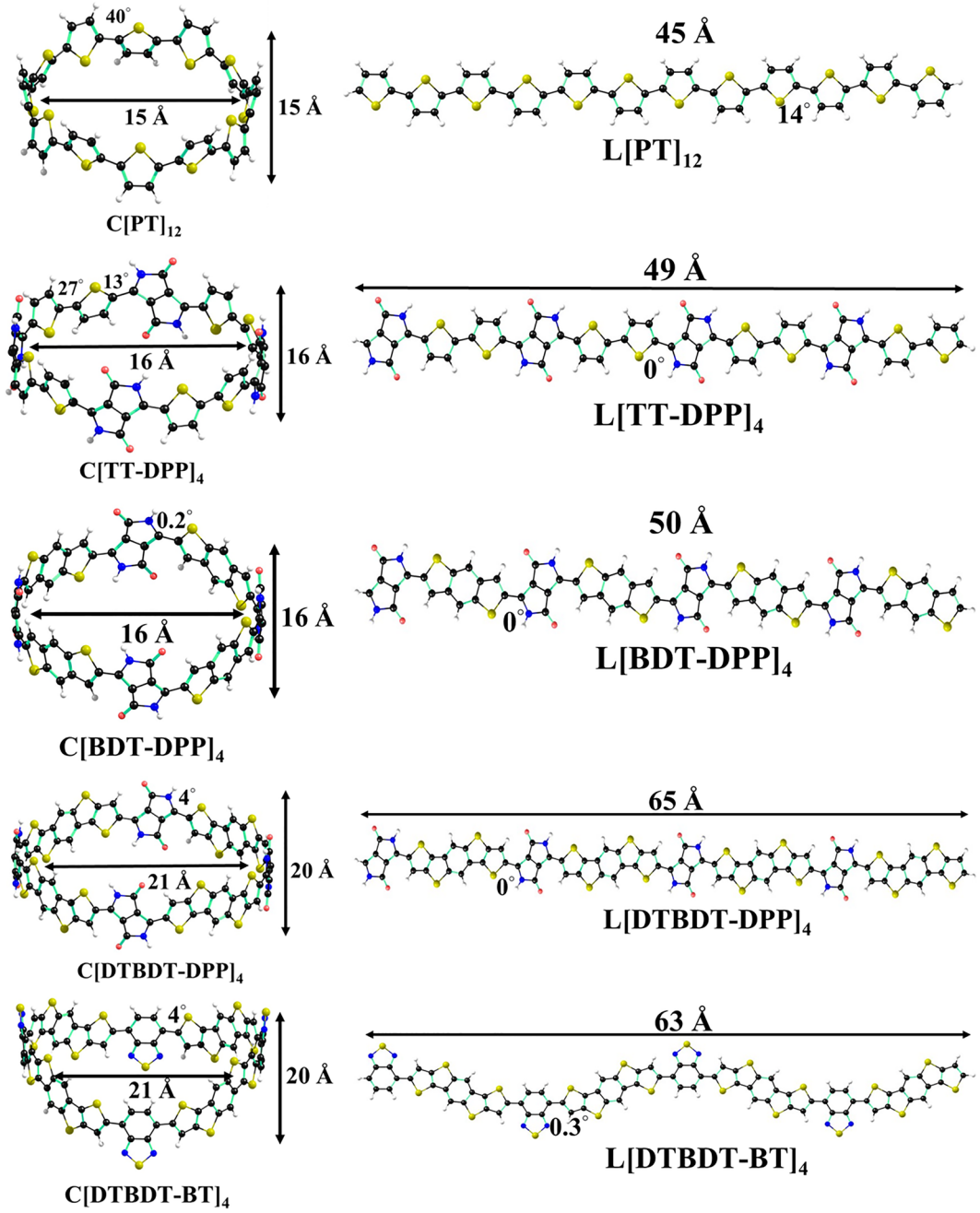

Figure 2. Optimized geometries of cyclic ($C[PT]_{12}$, $C[TT\text{-}DPP]_4$, $C[BDT\text{-}DPP]_4$, $C[DTBDT\text{-}DPP]_4$, and $C[DTBDT\text{-}BT]_4$) and linear ($L[PT]_{12}$, $L[TT\text{-}DPP]_4$, $L[BDT\text{-}DPP]_4$, $L[DTBDT\text{-}DPP]_4$, and $L[DTBDT\text{-}BT]_4$) donor–acceptor-based conjugated molecules as determined at B3LYP-D/6-31G(d,p) level of theory.

($L[TT\text{-}DPP]_n$, $L[BDT\text{-}DPP]_n$, $L[DTBDT\text{-}DPP]_n$, $L[DTBDT\text{-}BT]_n$). Again, in each case, we considered two, three, and four repeating units (n = 2, 3, and 4) for both cyclic and linear molecules.

Results and discussion

Geometry analysis. Optimized geometries of macrocyclic and linear compounds of $[PT]_{12}$, $[TT\text{-}DPP]_4$, $[BDT\text{-}DPP]_4$, $[DTBDT\text{-}DPP]_4$, and $[DTBDT\text{-}BT]_4$ are shown in Fig. 2, along with important dihedral angles obtained at B3LYP-D/6-31G(d,p) level of theory. Optimized geometries of smaller-size cyclic and linear compounds are depicted in Figs. S1 and S2. It can be seen from Fig. 2, Figs. S1 and S2 that the cyclic structures ($C[PT]_{12}$, $C[TT\text{-}DPP]_4$, $C[BDT\text{-}DPP]_4$, $C[DTBDT\text{-}DPP]_4$, and $C[DTBDT\text{-}BT]_4$), have twists in the dihedral angle (14°–18°) whereas linear oligomers ($L[PT]_{12}$, $L[TT\text{-}DPP]_4$, $L[BDT\text{-}DPP]_4$, $L[DTBDT\text{-}DPP]_4$, and $L[DTBDT\text{-}BT]_4$) have a co-planar backbone. $C[PT]_{12}$ exhibits larger dihedral angles between adjacent thiophenes among all macrocyclic compounds. The calculated dihedral angles between adjacent thiophenes range from 40° to 51°

Compound	Strain energy (kcal/mol)		
	n = 8	n = 10	n = 12
$C[PT]_n$	59.41	46.54	37.98
	n = 2	n = 3	n = 4
$C[TT\text{-}DPP]_n$	85.37	41.79	29.76
$C[BDT\text{-}DPP]_n$	85.89	54.07	38.87
$C[DTBDT\text{-}DPP]_n$	63.55	40.02	28.57
$C[DTBDT\text{-}BT]_n$	80.07	53.68	40.71

Table 1. Calculated strain energies (in kcal/mol) of designed macrocyclic molecules determined at B3LYP-D/6-31G** level of theory.

for $C[PT]_8$, $C[PT]_{10}$, and $C[PT]_{12}$ models. Linear polythiophenes ($L[PT]_8$, $L[PT]_{10}$, and $C[PT]_{12}$) have a planar structure with an end-to-end distance of 30 Å, 37 Å and 45 Å, respectively. On cyclization, $C[PT]_8$, $C[PT]_{10}$, and $C[PT]_{12}$ have a circular belt shape with diameters of 8 Å, 12 Å and 15 Å, respectively. In the case of TT-DPP-based compounds, linear oligomers ($L[TT\text{-}DPP]_2$, $L[TT\text{-}DPP]_3$, and $L[TT\text{-}DPP]_4$) have shown co-planar structures with the corresponding end-to-end distance of 24 Å, 36 Å and 49 Å, respectively. In the respective cyclic counterparts ($C[TT\text{-}DPP]_2$, $C[TT\text{-}DPP]_3$, and $C[TT\text{-}DPP]_4$), the values of dihedral angle between two thiophene rings are 5°, 17° and 27°. The dihedral angles between thiophene and DPP units are 1°, 17° and 34°, respectively. Similar to thiophene-based macrocycles, the donor–acceptor-based conjugated $C[TT\text{-}DPP)_n$ macrocycles also have the belt shape structure. The diameters of $C[TT\text{-}DPP]_2$, $C[TT\text{-}DPP]_3$, and $C[TT\text{-}DPP]_4$ are 8 Å, 12 Å and 16 Å, respectively.

Unlike thiophene-based macrocycles, $[BDT\text{-}DPP]_n$, $[DTBDT\text{-}DPP]_n$, and $[DTBDT\text{-}BT]_n$ have shown dihedral angle values close to 0°. Weak intermolecular interactions between oxygen atoms of DPP units and hydrogen atoms of BDT/DTBDT are responsible for smaller dihedral angles between the adjacent units. The absence of such interactions leads to twists in the dihedral angles in the cases of $C[PT]_n$. $C[BDT\text{-}DPP]_4$ has shown a circular shape with diameters of 16 Å; $C[BDT\text{-}DPP]_3$ formed a reuleaux triangle shape with a diameter of 12 Å, whereas $C[BDT\text{-}DPP]_2$ shows an oval shape with diameters of an 8 Å and 7 Å. Linear molecules of DTBDT-DPP ($L[DTBDT\text{-}DPP]_2$, $L[DTBDT\text{-}DPP]_3$, $L[DTBDT\text{-}DPP]_4$) show end-to-end lengths 32 Å, 49 Å and 65 Å. The top view of all optimized conjugated macrocycles is depicted in Fig. S3. The $C[DTBDT\text{-}DPP]_4$ macrocycle with four repeating units is arranged in a squircle (an intermediate shape between a square and a circle) shape with a diameter of 21 Å, whereas $C[DTBDT\text{-}DPP]_3$ forms a reuleaux triangle shape with a diameter of 16 Å. The smaller macrocycle $C[DTBDT\text{-}DPP]_2$ arranges in an oval shape (with a diameter of 12 Å and 10 Å). Due to the different morphology of the $[DTBDT\text{-}BT]_n$ backbone (n = 2–4), the linear oligomers show a zigzag arrangement of donor and acceptor units with diameters of 31 Å, 47 Å and 63 Å. Four repeating units of macrocyclic DTBDT-BT ring display a crown shape with a diameter of 20 Å, whereas $C[DTBDT\text{-}BT]_3$ arranged in a reuleaux triangle shape with a diameter of 15 Å, and $C[DTBDT\text{-}BT]_2$ shows an oval shape with diameters of 12 Å and 9 Å.

Strain energy. The energy associated with deforming a linear conjugated molecule when it is included in a conjugated macrocycle is defined as the macrocyclic strain energy (SE). SE in cyclic organic molecules arises due to the deviation in the structural parameters from their ideal angle to achieve maximum stability in a specific conformation. The SE arises due to the distortions of bond lengths and torsion angles from the typical values[32]. The energy associated with the formation of macrocyclic molecules from linear molecules is referred to as the macrocyclic strain energy[23,33]. The calculated strain energies for all the macrocyclic compounds using B3LYP-D/6-31G** are presented in Table 1. The calculated SE values of conjugated macrocycles are in the same range as the SE of previously reported macrocycles[16,32–35].

In cases of small and medium rings ($C[PT]_8$, $C[PT]_{10}$, two and three repetitive units of TT-DPP, BDT-DPP, DTBDT-DPP, and DTBDT-BT) exhibit higher strain energy due to bending of the coplanar aromatic structures. Larger macrocyclic rings $C[PT]_{12}$, $C[TT\text{-}DPP]_4$, $C[BDT\text{-}DPP]_4$, $C[DTBDT\text{-}DPP]_4$, and $C[DTBDT\text{-}BT]_4$ have less strain energies of 37.98, 29.76, 38.87, 28.57 and 40.71 kcal/mol, respectively. $C[TT\text{-}DPP]_4$ and $C[DTBDT\text{-}DPP]_4$ show less strain energy of 29.8 kcal/mol and 28.6 kcal/mol. The smaller strain energies in the case of $C[TT\text{-}DPP]_4$ is attributed to the presence of more dihedral angles between the adjacent rings. Having more dihedral angles provided conformational flexibility during cyclization. In the cases of other macrocycles, especially the D–A-based $C[BDT\text{-}DPP]_n$ and $C[DTBDT\text{-}BT]_n$ have fewer numbers of dihedral angles and larger fused aromatic rings. As a result, more molecules have to undergo more strain when they cyclize. Again, the lack of weak intermolecular interactions between thiophene units leads to more strain when the linear thiophene chain cyclizes. Smaller strain energy is observed in the squircle-shaped $C[DTBDT\text{-}DPP]_4$ ring (28.6 kcal/mol) compared to the crown-shaped $C[DTBDT\text{-}BT]_4$ ring (40.71 kcal/mol).

Radial π-conjugation. We have evaluated the highest occupied molecular orbital (HOMO) and the lowest unoccupied molecular orbital (LUMO) energies of $C[TT\text{-}DPP]_4$ and $L[TT\text{-}DPP]_4$ using three different functionals, viz., B3LYP, CAM-B3LYP, and mPW1PW91 functionals using the optimized geometries. The calculated results are compared with the previously reported experimental values (Table S1). We found that the mPW1PW91 functional can predict the HOMO and LUMO values comparable with the experimental values.

Thus, we have considered the mPW1PW91 functional to evaluate the frontier energy values for both linear and cyclic molecules.

HOMO, LUMO, and the difference between HOMO and LUMO energies (E_g) are the important factors that influence the optoelectronic properties and charge carrier transport properties of π-conjugated materials[20,36,37]. The pictorial representation of HOMO and LUMO wavefunctions obtained at the mPW1PW91/6-31G** level of theory for cyclic ($C[PT]_{12}$, $C[TT\text{-}DPP]_4$, $C[BDT\text{-}DPP]_4$, $C[DTBDT\text{-}DPP]_4$, and $C[DTBDT\text{-}BT]_4$) and linear ($L[PT]_{12}$, $L[TT\text{-}DPP]_4$, $L[BDT\text{-}DPP]_4$, $L[DTBDT\text{-}DPP]_4$, and $L[DTBDT\text{-}BT]_4$) molecules are depicted in Fig. 3. One can identify the difference in the π-electron distribution in cyclic and linear molecules. The radial π-conjugation can be observed in the cases of conjugated macrocycles, whereas the linear molecules show perpendicular π-conjugation. Also, except in the cases of $C[DTBDT\text{-}DPP]_4$ and $C[DTBDT\text{-}BT]_4$, in all other cyclic molecules, HOMO and LUMO wavefunctions are delocalized entire ring. Such delocalization indicates the formation of infinite radial π-conjugation. The HOMO delocalized on the entire ring, whereas the LUMO predominantly localized on acceptor units of $C[DTBDT\text{-}DPP]_4$ and $C[DTBDT\text{-}BT]_4$ (Fig. 3). Overall, replacing thiophene units with the electron-rich and electron-poor units in the conjugated macrocycles leads to fascinating electronic properties. In the cases of linear molecules, HOMO and LUMO wavefunctions are localized on a few repeating units. This suggests that the conjugated macrocycles systems can offer unique electronic and optical properties due to infinite π-conjugation and shape-persistent cycle structure compared to the conventional linear π-conjugated oligomers.

The calculated energies of HOMO–LUMO gaps and the energy difference between LUMO and LUMO + 1 for the larger systems are depicted in Fig. 4. The same energy values for all molecules considered in this study are reported in Table S2. Out of five systems considered in this study, we observed different electronic properties in the cases of PT and TT-DPP systems. We noted that HOMO energy levels are stabilized, and LUMO energy levels are destabilized when linear $L[PT]_{12}$ and $L[TT\text{-}DPP]_4$ molecules are cyclized (Fig. 4). In the $[BDT\text{-}DPP]_4$, $[DTBDT\text{-}DPP]_4$, and $[DTBDT\text{-}BT]_4$, both HOMO and LUMO wavefunctions are slightly stabilized when the linear one cyclizes.

Similarly, significant shrinkage in the HOMO–LUMO gaps is observed in the cases of $C[PT]_n$, $C[TT\text{-}DPP]_n$ systems when the size of the ring is increased. However, marginal or no changes in the HOMO–LUMO gaps are noted in the other systems. This reveals the intriguing property of radial π-conjugation. As both PT and TT-DPP-based conjugated rings exhibit more radial π-conjugation character, the electronic properties of these molecules are different from other cases. Also, as expected, variation in the HOMO, LUMO, and HOMO–LUMO gaps values are observed depending on the electron-donating and the electron-accepting nature of donor and acceptor units. Overall, the choice of donor and acceptor units impacts the radial π-conjugation character along with the energy level alteration. Also, a good correlation between the energy gap between LUMO and LUMO + 1 ($\Delta E_{(LUMO+1)\text{-}LUMO}$) of non-fullerene acceptors and power conversion efficiency (PCEs) is shown[37,38]. From Table S2, it is observed that in both linear and cyclic molecules designed, larger size compounds have the lower $\Delta E_{(LUMO+1)\text{-}LUMO}$ when compared to smaller size compounds. Moreover, the $\Delta E_{(LUMO+1)\text{-}LUMO}$ gap of larger cyclic compounds has similar values as linear compounds.

Reorganization energies. As described in the previous sections, the conjugated macrocycles offer unique electronic properties compared to linear counterparts due to the orientation of π-orbitals. Recent studies highlighted that the radially π-conjugated materials based on conjugated macrocycles could offer a much larger conductance modulation range than linear oligomers[39]. Thus, it is important to explore the charge transport properties of conjugated macrocycles. The internal reorganization energy (λ) is one of the key determinants of charge transport in organic materials[37,40–42]. The charge mobility exhibits an inverse relationship with reorganization energies, i.e., the lesser the λ value faster the charge mobility[20]. The calculated electron (λ_-) and hole (λ_+) reorganization energies for all the cyclic and linear compounds are listed in Table 2. The calculated hole and electron reorganization energy values for cyclic rings range from 0.09 to 0.26 eV and from 0.06 to 0.32 eV, respectively. The same values in linear oligomers range from 0.09 to 0.20 eV and from 0.06 to 0.19 eV, respectively. Slightly higher reorganization energies are observed in the cyclic structures than in the linear oligomers.

In the case of cyclic polythiophenes, λ_+ values are less than λ_- values. This indicates that the energy required for hole transfer is lower than the electron transfer process. It is observed that λ_- and λ_+ values for cyclic compounds are in good correlation with the size of the ring. Smaller λ_+ and λ_- values are observed in the larger rings and longer oligomers (Table 2). Reduction in λ_+ and λ_- values are found when one of the thiophene units is replaced with the DPP unit in both linear and cyclic compounds. Since the difference between λ_+ and λ_- values are marginal, cyclic/linear $[PT]_n$ and $[TT\text{-}DPP]_n$ can be used as ambipolar molecules. Replacement of bithiophene units (TT) with BDT ($C[BDT\text{-}DPP]_2$ to $C[BDT\text{-}DPP]_4$ and $L[BDT\text{-}DPP]_2$ to $L[BDT\text{-}DPP]_4$) leads to a reduction in λ_+ and λ_- values compared to linear and cyclic TT-DPP-based molecules. Furthermore, smaller λ_- values were noted than the λ_+ energies. A small increment in the λ_+ and λ_- values are observed when BDT unit replaced with DTBDT units ($C[DTBDT\text{-}DPP]_2$ to $C[DTBDT\text{-}DPP]_4$ and $L[DTBDT\text{-}DPP]_2$ to $L[DTBDT\text{-}DPP]_4$). Here also smaller λ_- values are noted than the λ_+ values. Further modification of DPP unit with BT ($C[DTBDT\text{-}BT]_2$ to $C[DTBDT\text{-}BT]_4$ and $L[DTBDT\text{-}BT]_2$ to $L[DTBDT\text{-}BT]_4$) results decreased λ_+ and λ_- values.

Open-circuit voltage. The open-circuit voltage (V*oc*) is an important factor in considering the device performance of any photovoltaic material and its operating mechanism. V*oc* can be explained as the entire quantity of current provided by the photovoltaic device without any external load for electricity generation[43,44]. The V*oc* is strongly related to fill factor and power conversion efficiency[45]. The V*oc* can be calculated by the following Eq.[46–48].

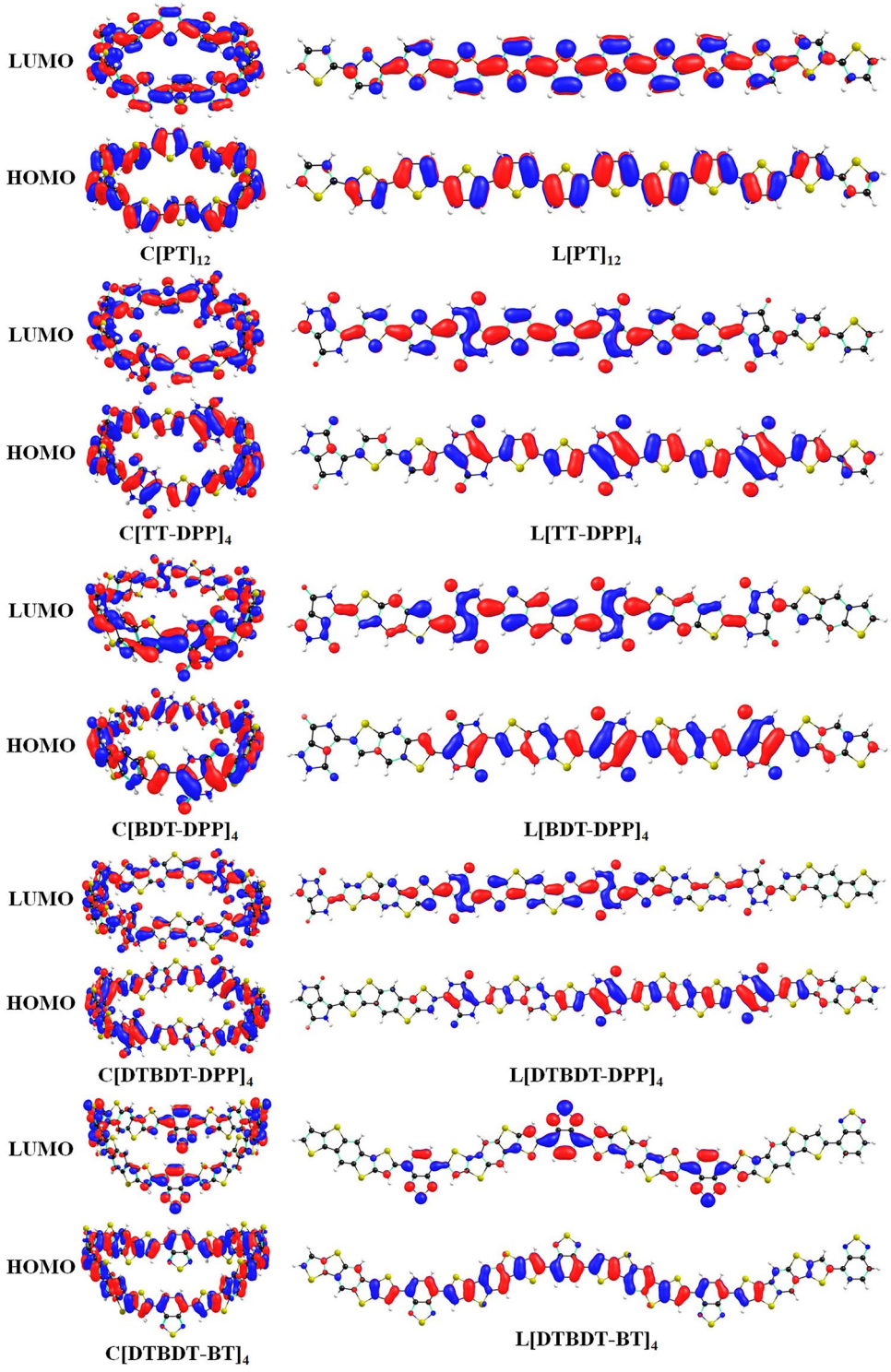

Figure 3. Pictorial representation of HOMO and LUMO wave functions of cyclic ($C[PT]_{12}$, $C[TT\text{-}DPP]_4$, $C[BDT\text{-}DPP]_4$, $C[DTBDT\text{-}DPP]_4$, and $C[DTBDT\text{-}BT]_4$) and linear ($L[PT]_{12}$, $L[TT\text{-}DPP]_4$, $L[BDT\text{-}DPP]_4$, $L[DTBDT\text{-}DPP]_4$, and $L[DTBDT\text{-}BT]_4$) molecules obtained at mPW1PW91/6-31G(d,p) level of theory.

$$V_{OC} = \frac{1}{e}(E_{HOMO}(D) - E_{LUMO}(A)) - 0.3 \quad (1)$$

Here, 0.3 is the voltage drop parameter, signifying that the open-circuit voltage can be more or less than 0.3, and e represents the element electron.

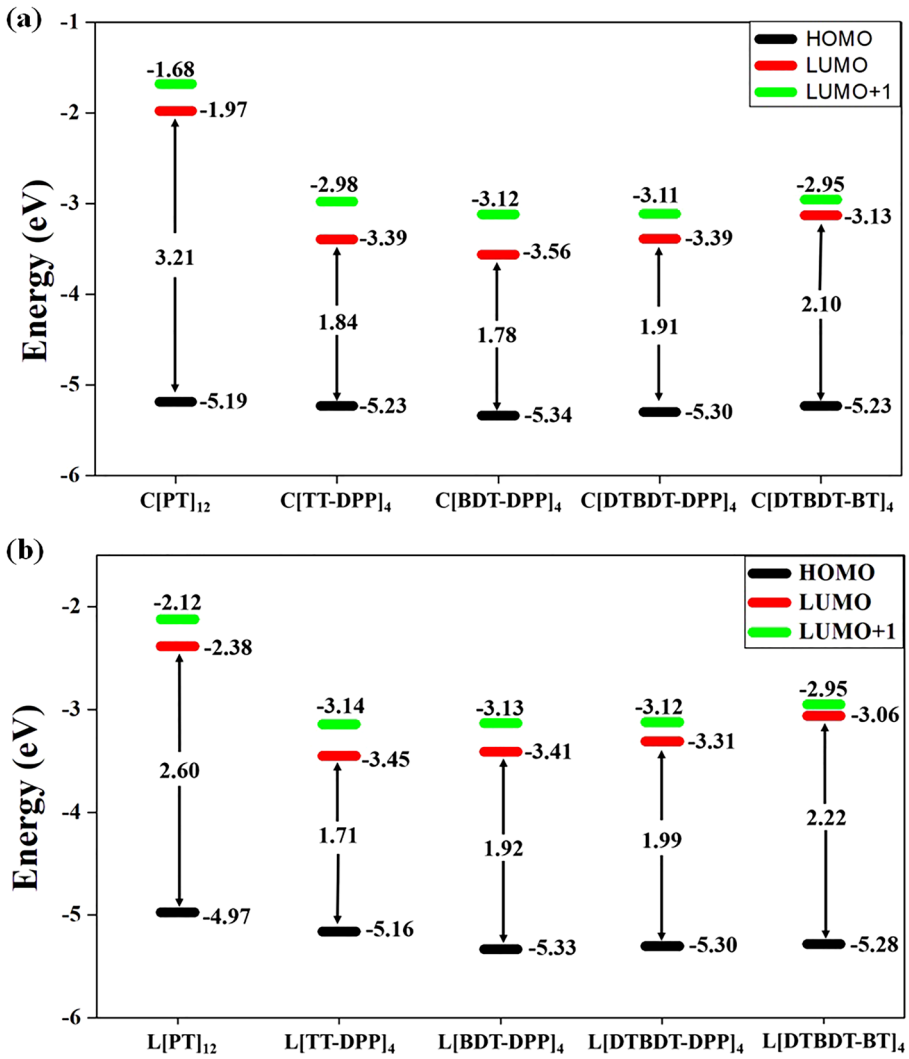

Figure 4. Calculated HOMO and LUMO energy levels of (**a**) cyclic ($C[PT]_{12}$, $C[TT\text{-}DPP]_4$, $C[BDT\text{-}DPP]_4$, $C[DTBDT\text{-}DPP]_4$, and $C[DTBDT\text{-}BT]_4$) and (**b**) linear ($L[PT]_{12}$, $L[TT\text{-}DPP]_4$, $L[BDT\text{-}DPP]_4$, $L[DTBDT\text{-}DPP]_4$, and $L[DTBDT\text{-}BT]_4$) donor–acceptor-based conjugated molecules determined at mPW1PW91/6-31G(d,p) level of theory. All values are in eV.

Usually, for successful exciton dissociation at the D–A interface and efficient CT acquisition from donor to acceptor, the energetic driving force (L_D-L_A), defined as the difference in LUMO energy between the donor and acceptor, should be more than 0.3 eV. By considering this criterion, calculated the V*oc* for designed macrocyclic compounds by considering linear and cyclic compounds as donor materials. The outcome of these parameters is presented in Figs. 5 and S4 and Table S3. All larger macrocyclic compounds have shown the acceptable V*oc* with $L[PT]_{12}$ and $C[PT]_{12}$ as donor materials. Among all combinations, $C[PT]_{12}$ as the donor and $C[DTBDT\text{-}BT]_4$ as the acceptor, and $L[PT]_{12}$ as the donor and $C[DTBDT\text{-}BT]_4$ as the acceptor, exhibit larger Voc of 1.76 V and 1.54 V respectively due to lower HOMO energy of $C[PT]_{12}$ and $L[PT]_{12}$ and higher LUMO of $C[DTBDT\text{-}BT]_4$. Two combinations, $L[DTBDT\text{-}BT]_4$ as the donor and $C[DTBDT\text{-}DPP]_4$ as the acceptor, $L[DTBDT\text{-}BT]_4$ as the donor and $C[TT\text{-}DPP]_4$ as the acceptor, have also shown a high V_{oc} of 1.6 V and 1.59 V. Based on these results, it is predicted that $C[DTBDT\text{-}BT]_4$ could be a promising acceptor material to enhance power conversion efficiency by virtue of better charge conduction properties.

Excited-state analysis. Time-dependent DFT (TD-DFT) calculations were carried out at the TD-mPW1PW91/6-31G(d,p) level of theory to elucidate the absorption properties of these molecules. The calculated optical properties of the five lowest excited states in cyclic rings (S_1–S_5) and the lowest excited state energies (S_1) of linear oligomers with their oscillator strength (f) are shown in Tables 3 and S4. In the cases of $C[PT]_{12}$, $C[TT\text{-}DPP]_4$, and $L[TT\text{-}DPP]_4$, the calculated absorption energies are in good agreement with the experimental reports[6,49].

As expected, shrinkage in the optical gaps is observed as the length of the oligomer increases. The calculated optical gaps in the $L[PT]_{12}$ and $L[TT\text{-}DPP]_4$ are 2.11 and 1.43 eV, respectively. The lowest absorption value is

Compound	Linear		Cyclic	
	λ_+	λ_-	λ_+	λ_-
$[PT]_8$	0.12	0.26	0.49	0.54
$[TT\text{-}DPP]_2$	0.23	0.20	0.36	0.40
$[BDT\text{-}DPP]_2$	0.20	0.18	0.28	0.21
$[DTBDT\text{-}DPP]_2$	0.09	0.07	0.21	0.16
$[DTBDT\text{-}BT]_2$	0.17	0.12	0.20	0.13
$[PT]_{10}$	0.23	0.22	0.35	0.41
$[TT\text{-}DPP]_3$	0.20	0.18	0.23	0.29
$[BDT\text{-}DPP]_3$	0.08	0.07	0.18	0.14
$[DTBDT\text{-}DPP]_3$	0.07	0.05	0.14	0.10
$[DTBDT\text{-}BT]_3$	0.12	0.09	0.13	0.09
$[PT]_{12}$	0.20	0.19	0.26	0.32
$[TT\text{-}DPP]_4$	0.12	0.11	0.17	0.21
$[BDT\text{-}DPP]_4$	0.10	0.08	0.13	0.11
$[DTBDT\text{-}DPP]_4$	0.16	0.15	0.10	0.07
$[DTBDT\text{-}BT]_4$	0.09	0.06	0.09	0.06

Table 2. Calculated energies (in eV) of hole (λ_+) and electron (λ_-) reorganization of cyclic and linear compounds (eV) calculated at B3LYP-D/6-31G** level of theory.

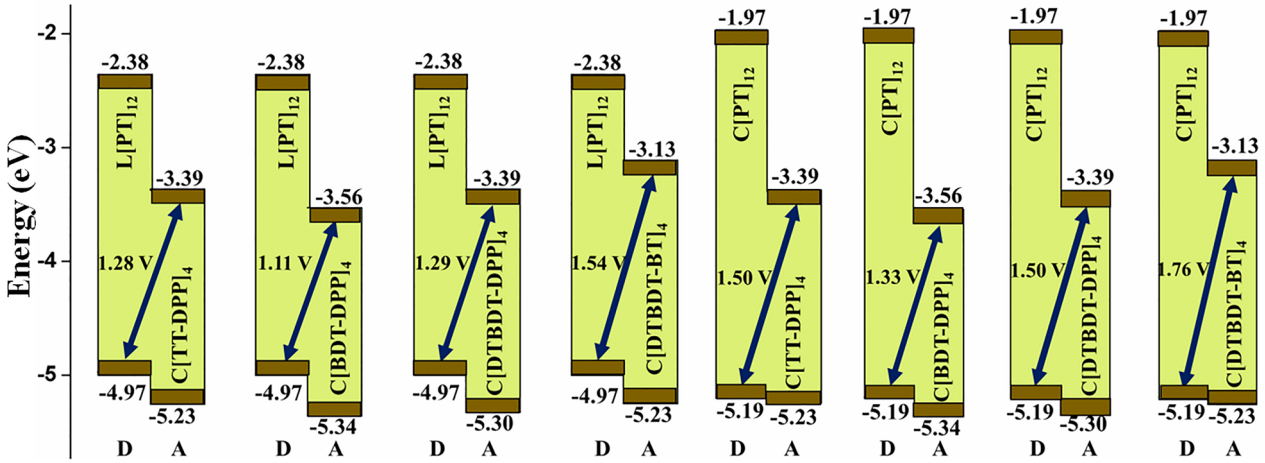

Figure 5. Open circuit voltage (V*oc*) of larger macrocyclic compounds with $L[PT]_{12}$ and $C[PT]_{12}$ as donor component.

substantially red-shifted ~ 300 nm when thiophene units are replaced with the DPP units. The introduction of DPP units stabilized the LUMO in $L[TT\text{-}DPP]_n$ oligomers. As a result, smaller optical gaps were observed in the DPP-based oligomers. Again, slight blue shifts in absorption values are observed when TT units are replaced with the electron-rich BDT/DTBDT units.

Strong blue-shift in the absorption energies are noted in the cyclic rings compared with the linear oligomers. The graphical representation of absorption wavelengths of larger linear and macrocyclic compounds is shown in Fig. 6. Macrocyclic compounds of TT-DPP, BDT-DPP, DTBDT-DPP, and DTBDT-BT show absorption at a longer wavelength (redshift) than their linear counterparts. The oscillator strength of macrocyclic compounds is zero by cyclization of linear compounds. One of the primary differences between cyclic and linear geometries is the degrees of freedom. The closed-loop formation by joining both termini reduces the degrees of freedom and conformational disorder. The lowest excited state excitation is forbidden for cyclic structures[50]. Thus, the lowest excitations in cyclic compounds originate from the $S_0 \geq S_2$ transitions.

Further, NTO analysis was carried out to characterize the nature of the excited state. The calculated hole and electron wavefunctions of larger cyclic and linear molecules are depicted in Figs. 7 and 8. The same for smaller oligomers is presented in Figs. S5–S8. The hole and electrons are delocalized across the backbone in the linear oligomers. Substantial overlap between hole and electron wavefunctions is observed in the lowest excited states of all oligomers. Thus, one can confirm that these states are Frenkel-type excitations (electron–hole pairs are localized at the single molecular unit). Strong oscillator strengths are also noted in all cases.

The lower excitation transitions are forbidden for conjugated macrocyclic compounds, unlike linear oligomers. Thus, we have evaluated the lowest five excited states using the TD-DFT method (Table S4). From these

	Cyclic				Linear	
	S_1	f	S_2	f	S_1	f
$[PT]_8$	3.08	0.64	3.67	0.64	2.33	2.78
$[TT\text{-}DPP]_2$	0.78	0.77	1.94	0.09	1.88	1.91
$[BDT\text{-}DPP]_2$	1.19	0.39	2.15	0.02	2.00	1.69
$[DTBDT\text{-}DPP]_2$	1.40	0.89	2.15	0.00	1.95	2.53
$[DTBDT\text{-}BT]_2$	1.41	0.36	1.97	0.23	1.99	1.54
$[PT]_{10}$	2.78	1.26	3.32	1.26	2.19	3.52
$[TT\text{-}DPP]_3$	1.49	1.10	2.16	0.01	1.58	3.09
$[BDT\text{-}DPP]_3$	1.27	1.04	1.99	0.04	1.84	2.94
$[DTBDT\text{-}DPP]_3$	1.46	1.75	2.02	0.04	1.74	3.99
$[DTBDT\text{-}BT]_3$	1.54	0.60	1.97	0.59	1.84	2.94
$[PT]_{12}$	2.58	1.82	3.04	1.82	2.11	4.25
$[TT\text{-}DPP]_4$	1.35	1.90	1.90	0.02	1.43	4.24
$[BDT\text{-}DPP]_4$	1.31	1.74	1.86	0.10	1.60	3.94
$[DTBDT\text{-}DPP]_4$	1.49	1.67	1.92	1.08	1.65	5.52
$[DTBDT\text{-}BT]_4$	1.62	1.60	1.93	1.60	1.78	4.15

Table 3. Calculated excited state energies (in eV) and oscillator strengths (au) of cyclic and linear molecules determined at mPW1PW91/6-31G** level of theory.

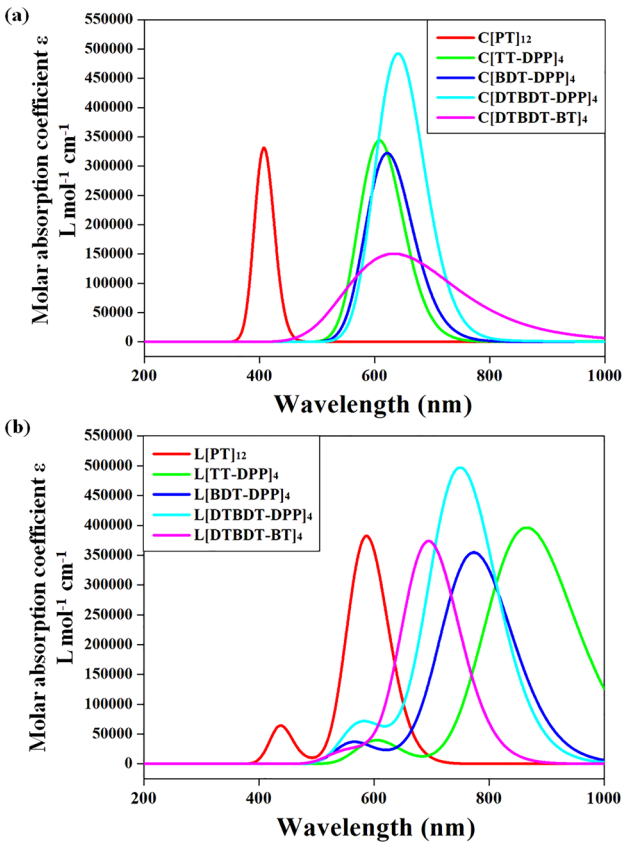

Figure 6. Graphical representation of absorption wavelengths of larger (**a**) linear and (**b**) macrocyclic compounds calculated at mPW1PW91/6-31G(d,p) level of theory.

calculations, we found the bright oscillator strengths in the second-excited state S_2 in the cases of $C[PT]_{12}$, $C[DTBDT\text{-}DPP]_4$, and $C[DTBDT\text{-}BT]_4$. $S_0 \geq S_4$ transition is predicted as a bright state in the cases of $C[TT\text{-}DPP]_4$ and $C[BDT\text{-}DPP]_4$. We have calculated the NTOs for these excitations to understand the nature of the excited state (Fig. S9). From Fig. S9, the NTO analysis on the S_2 state of $C[PT]_{12}$ and $C[DTBDT\text{-}DPP]_4$; and the S_4 state in $C[TT\text{-}DPP]_4$ and $C[BDT\text{-}DPP]_4$ indicate that the hole and electron wavefunctions are localized throughout the

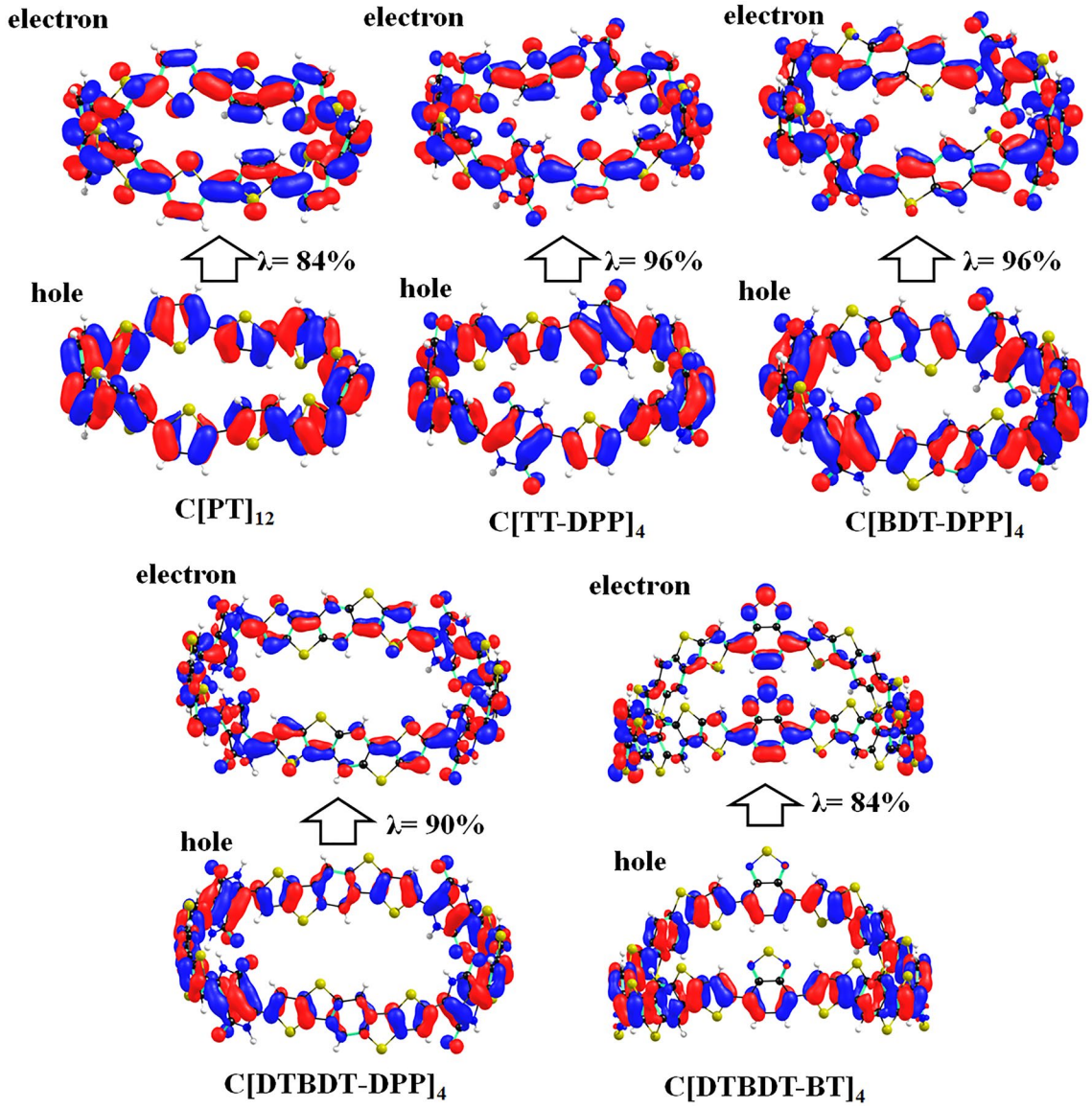

Figure 7. Pictorial representation of the natural transition orbitals of linear ($C[PT]_{12}$, $C[TT\text{-}DPP]_4$, $C[BDT\text{-}DPP]_4$, $C[DTBDT\text{-}DPP]_4$, and $C[DTBDT\text{-}BT]_4$) molecules corresponds to their lowest excited state (S_1) calculated at TD-mPW1PW91/6-31G(d,p) level of theory. Where, λ is the fraction of the hole–electron contribution to the excitation.

compound which refers Frenkel-type excitations. In $C[DTBDT\text{-}BT]_4$, the second excited state exhibits hybridized local and charge-transfer (HLCT) state. Here, the hole wavefunction is delocalized on entire molecule and electron wavefunction is dominantly localized on two opposite BT acceptor units."

Exciton binding energy and singlet–triplet gap. The singlet–triplet energy gap (ΔE_{ST}), which is the energy difference between the lowest non-charge transfer singlet (S_1) and triplet (T_1) excited states, is an important parameter for OSC material. The exciton dissociation process occurs through singlet-CT states. Nongeminate or bimolecular recombination may occur during charge migration; this results in the creation of CT excitons, which can be of singlet or triplet character. Through back electron transfer triplet-CT, the state relaxes to the T_1 state, and recombination occurs. Due to the large difference between CT state energy and T_1 energy, the speed of T_1 to thermalize back into triplet-CT will be limited if the CT driving force is small (as required to maximize open-circuit voltage, V_{OC}). In order to reduce both voltage loss and nongeminate recombination, the ΔE_{ST} needs to be minimized[51,52]. The calculated ΔE_{ST} values for larger macrocyclic and linear compounds are included in Table 4. Indeed, from Table 4, the energies of S_1 and T_1 of macrocyclic compounds are lower than corresponding linear compounds, thus reducing the ΔE_{ST} in macrocyclic compounds (~0.41 to 0.49 eV) compared to linear (~0.46 to 0.67 eV). Among macrocyclic compounds $C[TT\text{-}DPP]_4$ and $[DTBDT\text{-}BT]_4$ consists of lower ΔE_{ST} of 0.41 eV and 0.43 eV. As a result, it appears that cyclization of linear compounds can effectively minimize voltage loss and nongeminate recombination by lowering the ΔE_{ST}.

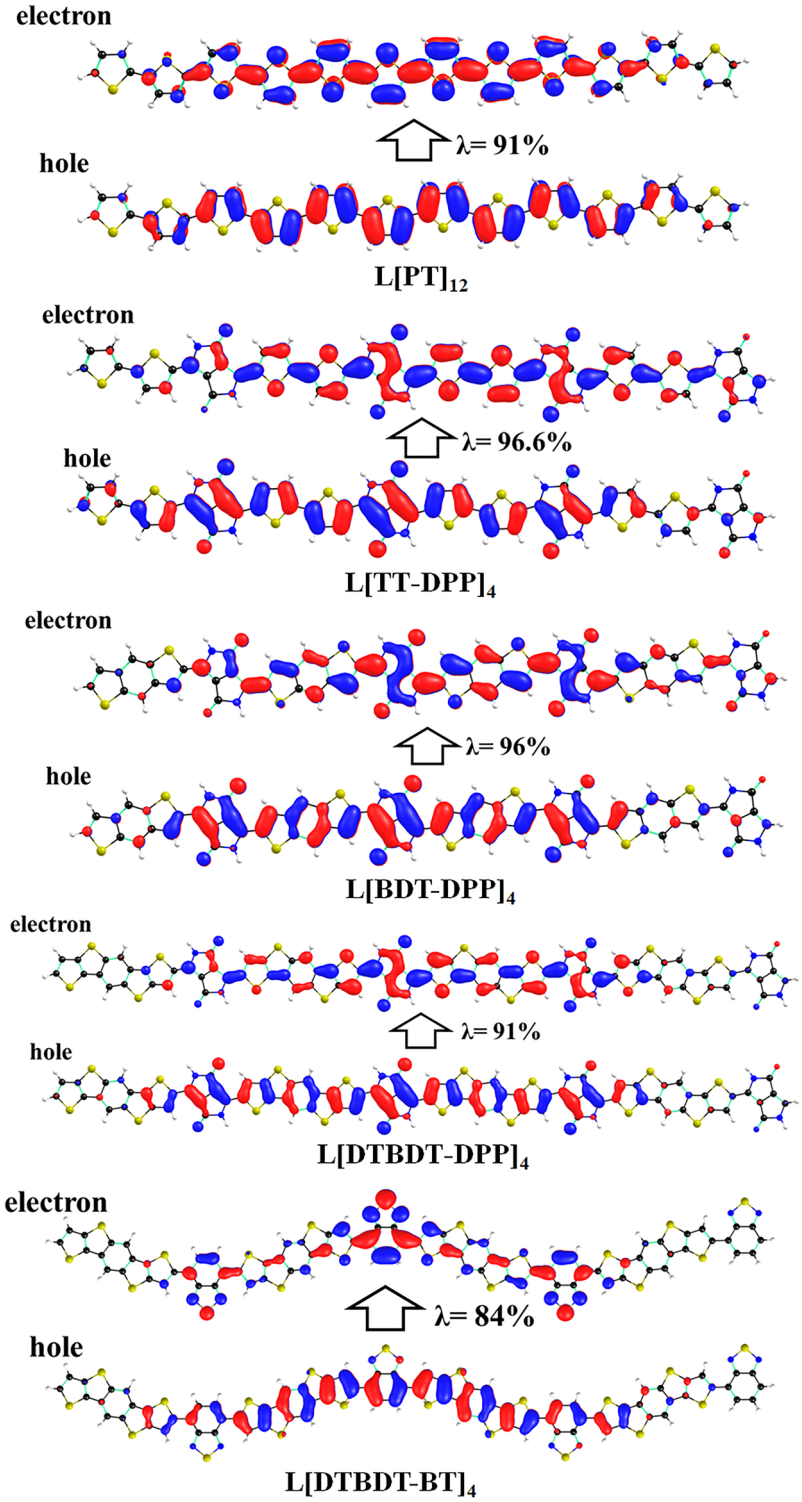

Figure 8. Pictorial representation of the natural transition orbitals of linear ($L[PT]_{12}$, $L[TT\text{-}DPP]_4$, $L[BDT\text{-}DPP]_4$, $L[DTBDT\text{-}DPP]_4$, and $L[DTBDT\text{-}BT]_4$) molecules corresponds to their lowest excited states (S_1) calculated at TD-mPW1PW91/6-31G(d,p) level of theory. Where, λ is the fraction of the hole–electron contribution to the excitation.

Further, the exciton separation procedure leads to additional energy losses because of the high exciton binding energy E_b. Large exciton binding energy must be overcome to dissociate exciton to charges successfully[44,46,53]. To overcome this, one of the key parameters is E_b, which is directly related to the charge separation in OSCs. It can be calculated theoretically using following expression[44,52,54].

	Cyclic				Linear			
	S_1	E_b	T_1	ΔE_{ST}	S_1	E_b	T_1	ΔE_{ST}
$[PT]_{12}$	2.58	0.63	2.09	0.49	2.11	0.48	1.52	0.59
$[TT\text{-}DPP]_4$	1.35	0.49	0.94	0.41	1.43	0.28	0.81	0.62
$[BDT\text{-}DPP]_4$	1.31	0.47	0.88	0.44	1.60	0.32	0.93	0.67
$[DTBDT\text{-}DPP]_4$	1.49	0.42	1.00	0.48	1.65	0.33	1.01	0.64
$[DTBDT\text{-}BT]_4$	1.62	0.48	1.19	0.43	1.78	0.44	1.33	0.46

Table 4. Calculated lowest singlet (S_1), triplet (T_1) excitation energies, Singlet–triplet gap ΔE_{ST} and exciton binding energy E_b of larger macrocyclic and linear compounds in eV obtained at mPW1PW91/6-31G** level of theory.

Compound	HOMO–HOMO coupling (meV)	LUMO–LUMO coupling (meV)
$C[PT]_{12}$	16.96	16.68
$C[TT\text{-}DPP]_4$		
AA	17.92	18.31
DA	1.01	0.87
DD	18.49	28.38
$C[BDT\text{-}DPP]_4$		
AA	27.81	13.32
DA	1.73	3.85
DD	6.13	12.36
$C[DTBDT\text{-}DPP]_4$		
AA	18.34	16.16
DA	13.84	16.30
DD	17.78	17.60
$C[DTBDT\text{-}BT]_4$		
AA	7.63	31.20
DA	19.04	12.32
DD	13.88	3.74

Table 5. Calculated transfer integral values (in meV) between conjugated macrocycles at B3LYP/6-31G** level of theory.

$$E_b = IP - EA - E_{opt} \quad (2)$$

Where IP and EA are the ionization potential and electron affinity, respectively; and E_{opt} is the optical band gap.

The E_b of larger macrocyclic and linear compounds were calculated and given in Table 4. The table showed that macrocyclic compounds showed little more E_b values of difference ~ 0.14 to 0.2 eV when compared to linear compounds. Among the designed macrocyclic compounds, C[DTBDT-DPP]4, C[BDT-DPP], and C[DTBDT-BT]4 possess the lower E_b.

Electronic coupling. The charge transfer properties of organic molecules are primarily determined by lower reorganization energy and electronic coupling between molecules. The HOMO–HOMO coupling accelerates hole transport, whereas the LUMO–LUMO coupling enhances the electron transport. We evaluated the electronic couplings of dimer configurations of macrocyclic compounds in three packing arrangements. The first packing mode is the interaction of an acceptor unit of one macrocyclic ring with the acceptor unit of another ring (AA). The second packing mode corresponds to the acceptor unit of one ring interacting with the donor unit of another ring (AD). And the third packing mode is the donor unit of one ring with the donor unit of another ring (DD) (Fig. S10). The distance between the rings is fixed at 3.5 Å in all complexes. All transfer integral values are calculated using the B3LYP/6-31G(d,p) level of theory. All the findings of electronic coupling values are tabulated in Table 5. In the case of $C[PT]_{12}$, we found similar HOMO–HOMO and LUMO–LUMO electronic coupling values. Also, we note lower reorganization energies (λ_+ and λ_-) are observed (Tables 2 and 5). Therefore $C[PT]_{12}$ can be categorized as an ambipolar molecule. Modifying the thiophene unit with the DPP acceptor unit ($C[TT\text{-}DPP]_4$) enhanced the LUMO–LUMO coupling in DD interacting configuration, whereas weaker coupling was observed in the DA configuration. In the case of $C[BDT\text{-}DPP]_4$, substantial HOMO–HOMO coupling was seen in the AA configuration, whereas weak coupling was observed in the DA configuration. In the instance of $[DTBDT\text{-}DPP]_4$, it has shown similar HOMO–HOMO and LUMO–LUMO coupling in all (AA, DA, and DD) configurations. Based on electronic coupling values and reorganization energies, one can

	r (Å)	k_h	μ_h	k_e	μ_e
$C[PT]_{12}$	3.5	1.55×10^{12}	0.04	3.82×10^{11}	0.01
$C[TT\text{-}DPP]_4$					
AA	3.5	2.53×10^{12}	0.06	1.54×10^{12}	0.04
DA	3.5	7.80×10^{9}	0.00	4.75×10^{9}	0.00
DD	3.5	2.53×10^{12}	0.06	3.73×10^{12}	0.09
$C[BDT\text{-}DPP]_4$					
AA	3.5	1.03×10^{13}	0.25	2.94×10^{12}	0.07
DA	3.5	5.26×10^{10}	0.00	2.78×10^{11}	0.01
DD	3.5	4.74×10^{11}	0.01	2.50×10^{12}	0.06
$C[DTBDT\text{-}DPP]_4$					
AA	3.5	6.51×10^{12}	0.16	8.23×10^{12}	0.20
DA	3.5	3.94×10^{12}	0.09	8.23×10^{12}	0.20
DD	3.5	6.51×10^{12}	0.16	1.04×10^{13}	0.25
$C[DTBDT\text{-}BT]_4$					
AA	3.5	1.49×10^{12}	0.04	3.68×10^{13}	0.88
DA	3.5	8.42×10^{12}	0.20	5.51×10^{12}	0.13
DD	3.5	4.57×10^{12}	0.11	6.12×10^{11}	0.01

Table 6. Calculated hole and electron charge transport rate constant k_h/k_e (S^{-1}), hole and electron mobility μ_h/μ_e ($cm^2\ V^{-1}\ S^{-1}$) using coupling values obtained from three different packing configurations of macrocyclic compounds with charge transport distance r (Å) between two macrocycles, obtained with Eq. (6) and (7).

confirm the ambipolar behavior of $[DTBDT\text{-}DPP]_4$. When it comes to $[DTBDT\text{-}BT]_4$, the electronic coupling values depend on the packing between the rings. More significant LUMO–LUMO coupling was observed in the AA configuration, and weaker LUMO–LUMO coupling was observed in the DD configuration. $C[TT\text{-}DPP]_4$ and $[DTBDT\text{-}BT]_4$ can act as electron acceptor materials based on strong LUMO–LUMO couplings and low electron reorganization energies. However, the molecular packing of macrocyclic molecules strongly influences the electronic coupling properties.

The hole/electron mobility. The intermolecular packing configurations of adjacent molecular segments have a considerable impact on the transfer integral. It has been widely reported that face-to-face parallel-stacking has greater orbital overlapping, resulting in a large-scale contribution to charge transfer in organic systems. To estimate the charge transport rate constants (k_h and k_e) and mobilities (μ_h and μ_e), we have considered in three packing configurations (Fig. S10) as described above in electronic coupling calculations. Hole and electron transport rate constant calculated using Eq. (6) and hole and electron mobilities calculated using Eq. (7) for different configuration of packings of larger macrocyclic compounds are tabulated in Table 6. From this table one can observe that the mode of packing configuration impacted the hole and electron rate constants and mobilities. Increasing the conjugation length in macrocyclic compounds increases the rate of mobilities of hole and electron. Among the macrocyclic compounds $C[DTBDT\text{-}BT]_4$ showing the highest k_e and μ_e of $3.68\times10^{13}\ S^{-1}$ and 0.88 $cm^2\ V^{-1}\ S^{-1}$ due to highest LUMO–LUMO coupling and lower electron reorganization energy in AA configuration. As well in DA configuration it is showing hole transport rate of $8.42\times10^{12}\ S^{-1}$ and hole mobility 0.2 $cm^2\ V^{-1}\ S^{-1}$. Among the macrocyclic compounds $C[BDT\text{-}DPP]_4$ consists of high hole transport rate $1.03\times10^{13}\ S^{-1}$ and hole mobility 0.25 $cm^2\ V^{-1}\ S^{-1}$.

Properties of electron-donor and electron-acceptor blends. It is clear from the discussion in previous sections that the conjugated D–A macrocycles can indeed be used as electron acceptor materials (similar to fullerenes and fullerene derivatives) for organic solar cell applications. We have constructed a model interface between electron donor ($L[PT]_{12}$) and electron acceptor materials. The $L[PT]_{12}$ and conjugated D–A macrocycles complexes are considered to gain insights into molecular packing at the interface, charge transfer states, and charge separation behavior. $C[TT\text{-}DPP]_4$, $C[BDT\text{-}DPP]_4$, $C[DTBDT\text{-}DPP]_4$, and $C[DTBDT\text{-}BT]_4$ have been selected as acceptor materials and $L[PT]_{12}$ selected as donor material to model linear-cyclic interfaces. Further, these results are compared with the complexes which are made from linear oligomers. $L[BDT\text{-}DPP]_4$ and $L[PT]_{12}$ are considered as electron-acceptor and electron-donor materials, respectively. All the complexes were optimized at the B3LYP-D/6-31G(d,p) level of theory. Further, the excited state analysis was carried out on the ground-state optimized geometries. NTO analysis was also performed to understand the nature of excitation transition. One of the drawbacks of OSCs is that exciton lifetimes are typically very short due to the involvement of coulombically bound electron–hole pairs, resulting in short exciton diffusion lengths. Thus, an adequate driving force for charge separation is required for complete electron and hole separation. The spatial distance between the centroid of the hole and electron ($\Delta r_{h\text{-}e}$), which is the key factor in charge separation, is obtained by the Multiwfn code[55]. Pictorial representation of charge-transfer states of all complexes and CT state energies and $\Delta r_{h\text{-}e}$ values are shown in Fig. 9. Larger $\Delta r_{h\text{-}e}$ values are observed in the complexes where linear electron-

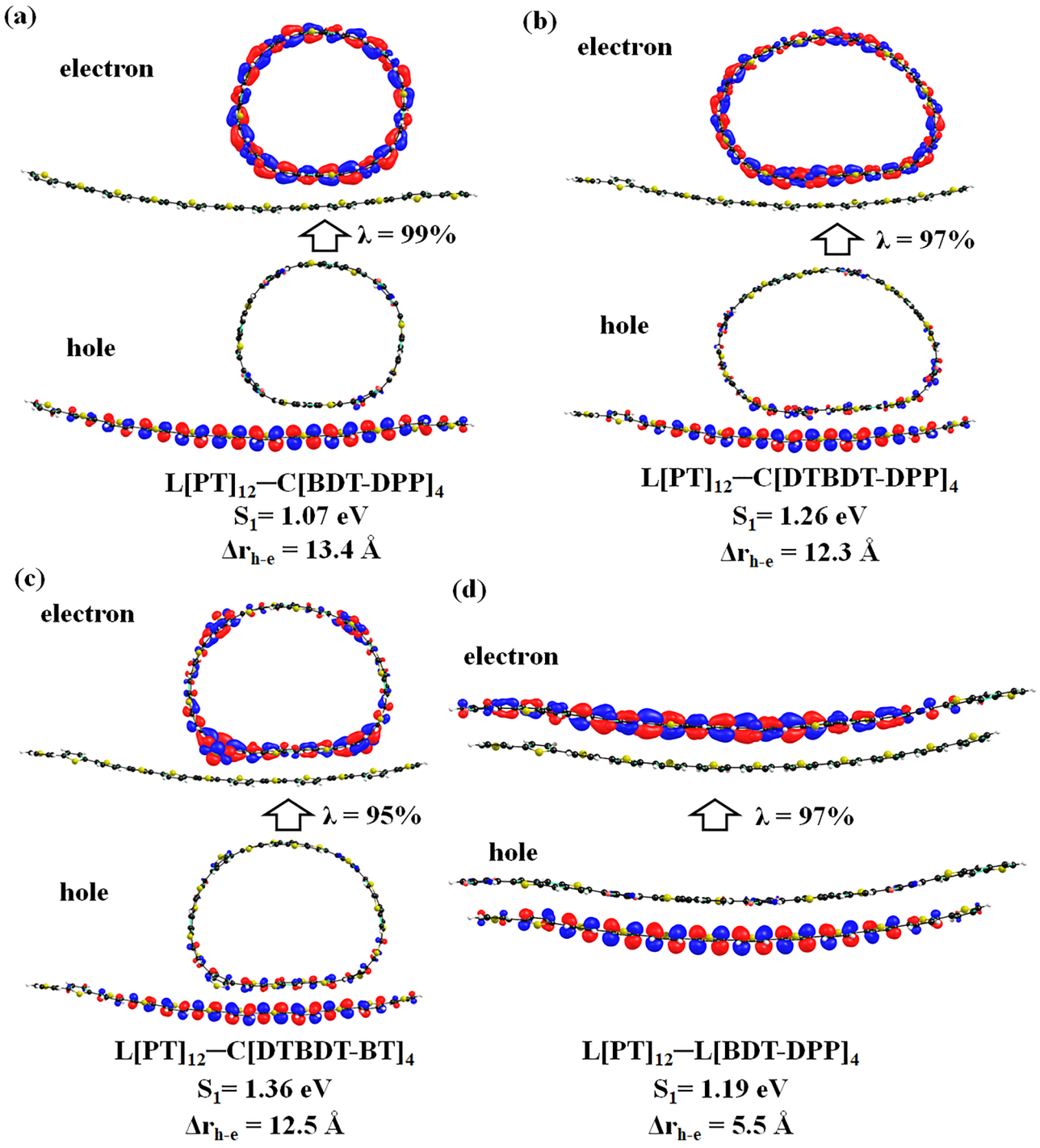

Figure 9. Pictorial representation of the charge transfer states of various cyclic-linear complexes (**a**) $L[PT]_{12}$—$C[BDT\text{-}DPP]_4$, (**b**) $L[PT]_{12}$—$C[DTBDT\text{-}DPP]_4$, (**c**) $L[PT]_{12}$—$C[DTBDT\text{-}BT]_4$ and linear–linear complex **(d)** $L[PT]_{12}$—$L[BDT\text{-}DPP]_4$ calculated at TD-B3LYP-D/6-31G(d,p) level of theory where λ is the fraction of the hole–electron contribution to the excitation.

donor and cyclic electron-acceptor is considered. The electron wavefunction is delocalized away due to the cyclic structure of the acceptor molecule. As a result, a more significant $\Delta r_{h\text{-}e}$ distance (~ 12–13 Å) in linear-acceptor complexes is observed. Among all interfaces, $L[PT]_{12}$—$C[BDT\text{-}DPP]_4$ showed the highest $\Delta r_{h\text{-}e}$ of 13.4 Å. The DTBDT unit containing macrocyclic compounds exhibited more structural distortion when interacting with donor material. Hence less $\Delta r_{h\text{-}e}$ when compared to $C[BDT\text{-}DPP]_4$. In the case of linear electron-donor and linear electron-acceptor complexes, due to one-on-one packing, strong Coulomb interactions lead to a smaller $\Delta r_{h\text{-}e}$ of 5.5 Å.

The calculated hole and electron charge transfer rates and rate of charge recombination (using Eq. (9)) of modeled interfaces are given in Table 7, along with free energy changes ΔG_{CT} and ΔG_{CR}. The negative ΔG_{CT} and

D/A complex	ΔG_{CT}	ΔG_{CR}	λ	$V_{H\text{-}H}$	$V_{L\text{-}L}$	$V_{H\text{-}L}$	k_{CT} hole	k_{CT} electron	k_{CR}
$L[PT]_{12}/C[TT\text{-}DPP]_4$	− 0.53	− 1.58	0.51	0.002	0.002	0.02	9.34×10^{11}	9.34×10^{12}	3.09×10^{3}
$L[PT]_{12}/C[BDT\text{-}DPP]_4$	− 0.70	− 1.41	0.46	0.003	0.031	0.05	6.59×10^{10}	6.59×10^{10}	3.19×10^{5}
$L[PT]_{12}/C[DTBDT\text{-}DPP]_4$	− 0.53	− 1.59	0.45	0.004	0.076	0.02	3.49×10^{11}	1.33×10^{14}	6.31
$L[PT]_{12}/C[DTBDT\text{-}BT]_4$	− 0.27	− 1.84	0.44	0.005	0.099	0.01	3.34×10^{11}	1.06×10^{14}	3.8×10^{-7}
$L[PT]_{12}/L[BDT\text{-}DPP]_4$	− 0.55	− 1.56	0.47	0.003	0.002	0.02	1.93×10^{11}	6.20×10^{10}	2.05×10^{2}

Table 7. Calculated free energy change of charge transfer ΔG_{CT} (eV) and charge recombination ΔG_{CR} (eV), reorganization energy λ (eV), transfer integrals HOMO–HOMO coupling $V_{H\text{-}H}$ (eV), LUMO–LUMO coupling $V_{L\text{-}L}$ (eV), HOMO–LUMO coupling $V_{H\text{-}L}$ (eV), rate of charge transfer (k_{CT}) and charge recombination (k_{CR}) in S^{-1} mPW1PW91/6-31G** level of theory.

ΔG_{CR} values demonstrate that charge transfer and charge recombination are thermodynamically favourable processes. An ideal electron-donor and electron-acceptor interface should have a higher value of k_{CT} and lower k_{CR} to enable effective exciton dissociation and reduced charge recombination at the interface. To emphasize this the ratio of k_{CT}/k_{CR} are also calculated. The ratio of hole k_{CT}/k_{CR} followed the order $C[DTBDT\text{-}BT]_4 > C[DTBDT\text{-}DPP]_4 > C[TT\text{-}DPP]_4 > C[BDT\text{-}DPP]_4$. The same order is also observed in the case of the ratio of electron $k_{CT}/k_{CR.}$ As per Marcus' theory, reorganization energy and electronic coupling are the two factors which influence the charge transfer rate. Strong LUMO–LUMO coupling is observed in the cases of $C[DTBDT\text{-}BT]_4$ and $C[DTBDT\text{-}DPP]_4$ when compared to other complexes leads to high charge transfer rates. The lowest charge recombination rate in $L[PT]_{12}$—$C[DTBDT\text{-}BT]_4$ results in the high k_{CT}/k_{CR} ratio of 2.7×10^{20}. Overall, the combination of $L[PT]_{12}$—$C[DTBDT\text{-}BT]_4$ and $L[PT]_{12}$—$C[DTBDT\text{-}DPP]_4$ has a stronger exciton dissociation and easier CT among all interfaces considered and thus can be considered as a promising combination of electron-donor and electron-acceptor materials.

Conclusions

In conclusion, we have demonstrated the geometrical, electronic, and optical properties of new donor–acceptor-based conjugated macrocycle molecules using DFT and TD-DFT methodologies. The newly designed macromolecules show promising electronic properties due to radial π-conjugation. The choice of donor and acceptor units strongly influences the geometrical, electronic, and excited-state properties. The strain energy in the macrocyclic compounds decreases with the size of the ring. Introducing electron-rich and electron-poor units impacted the radial π-conjugation character along with the HOMO–LUMO energy level alteration. Designed molecules can be used as ambipolar as the hole and electron reorganization energies have marginal differences. Among all the designed macrocycles, large size compounds $C[TT\text{-}DPP]_4$, $C[BDT\text{-}DPP]_4$, $C[DTBDT\text{-}DPP]_4$, and $C[DTBDT\text{-}BT]_4$ can be used as electron acceptor materials for organic solar cell applications. The charge transfer integral values strongly depend on the packing configuration of dimers. Furthermore, we have also studied the interface properties between linear-cyclic and linear–linear complexes considering $L[PT]_{12}$ as the donor component. Due to cyclization, the spatial distance between hole and electron in linear-cyclic complexes is doubled compared to the linear–linear complex, which can act as efficient materials for charge separation and can be potential molecules for organic solar cell applications. Based on various opto-electronic properties and charge transfer rate and charge recombination rate $C[DTBDT\text{-}BT]_4$ shown better performance in electron transport and exciton separation.

Materials and methods

The geometries of neutral and charged macrocyclic molecules and corresponding linear counterparts were optimized using density functional theory (DFT) based B3LYP/6-31G(d) method with dispersion correction. Further, single-point calculations were carried out to calculate optical and electronic properties using various DFT methods such as CAM-B3LYP and mPW1PW91 using the optimized geometries. In order to understand the strain in macrocyclic molecules, strain energies were calculated using B3LYP-D functional with the 6-31G(d,p) basis set. Excited-state analyses were performed using optimized geometries at TD-B3LYP/6-31G(d,p), TD-CAM-B3LYP/6-31G(d,p), and TD-mPW1PW91/6-31G(d,p) level of theory. Natural Transition Orbital (NTO) analysis was carried out to understand the nature of excited states[56]. All calculations were performed using the Gaussian16 package[57].

The charge transport process in nonordered semiconductors can be explained using an incoherent hopping mechanism[40,46,58]. In the hopping mechanism, charge transfer occurs in sequential jumps between adjacent molecules[40,59,60]. Thus, the charge transfer rate can be described using Marcus theory. It is well known from the rate expression that the reorganization energy influences the rate of charge transfer[42,59,61–63]. Therefore, both hole and electron reorganization energies (λ_+ and λ_-) were calculated by using the following Eqs. (3) and (4)[47].

$$\lambda_+ = E^+(M^0) - E^+(M^+) + E^0(M^+) - E^0(M^0) \tag{3}$$

$$\lambda_- = E^-(M^0) - E^-(M^-) + E^0(M^+) - E^0(M^0) \tag{4}$$

Where E^0, E^+, and E^- represents energy of neutral, cationic, and anion respectively and M^0, M^+, and M^- represents optimized geometries of neutral, cationic, and anion systems respectively.

The total strain energy (E_{Strain}) in a macrocyclic compound is calculated using the following Eq. (5)[33,64].

$$E_{Strain} = \left(E_{Macrocycle} + E_{Cap}\right) - E_{Linear} \tag{5}$$

At ambient temperature, the charge transport in organic solar cells is likely to occur through the thermally activated hopping model. In this model, the charge carriers localize on a single molecule and hop from one molecule to the adjacent molecule. The charge transfer rate constant (k) between equivalent neighbouring molecules can be defined by semiclassical Marcus theory. The charge transfer rate constant can be expressed as follows (the free energy difference (ΔG) for the self-exchange CT reaction process is neglected)[52,65,66].

$$k = \frac{2\pi}{\hbar} V^2 \left(\frac{1}{\sqrt{4\pi\lambda k_B T}}\right) \exp\left(-\frac{\lambda}{4k_B T}\right) \tag{6}$$

Where k is the rate of charge transfer for hole and electron (k_h and k_e respectively), V electronic coupling of the hole and electron transfer (V_h and V_e) computed with the generalized Mulliken–Hush (GMH) method[44,67]. ħ is Planck's constant, k_B is the Boltzmann constant, T is room temperature, and λ is the hole and electron reorganization energy (λ_h and λ_e) of the charge transfer process calculated using Eqs. (3) and (4).

Further, to gain insights into impact of molecular modifications on the electron mobility (μ) in these newly designed NFAs, the Einstein–Smoluchowski equation is used estimate the drift mobility of hopping μ using given as follows[68,69].

$$\mu = \frac{e}{k_B T} D \tag{7}$$

where μ is the mobility of hole and electron (μ_h and μ_e), e is the electron charge, k_B is the Boltzmann constant, T is room temperature, and D is the diffusion coefficient which can be expressed in terms of the charge transfer rate constant k and r (the distance between two centroids of backbones of two molecules in one dimer) as follows:

$$D = \frac{1}{2} k r^2 \tag{8}$$

Charge transfer at the donor–acceptor interface is the process by which an electron/hole of the donor/acceptor injects into the acceptor/donor after local excitation. Charge transfer at the interface in the modeled D/A systems can be roughly interpreted as electron/hole transfer driven by the donor/acceptor local excitation states. The rate of charge transfer (k_{CT}) and charge recombination (k_{CR}) in D/A systems can be evaluated by the Marcus theory as follows[65].

$$k = \frac{2\pi}{\hbar} |V_{DA}|^2 \left(\frac{1}{\sqrt{4\pi\lambda k_B T}}\right) \exp\left(-\frac{(\Delta G + \lambda)^2}{4\lambda k_B T}\right) \tag{9}$$

Where k is the rate constant for charge transfer (k_{CT}) and charge recombination (k_{CR}), V_{DA} represents the CT integral between the donor and acceptor estimated using the GMH model, λ is the reorganization energy (internal and external), k_B is the Boltzmann constant, T is temperature, and ΔG is the free energy change for electron transfer process. The ΔG during the CT process is denoted as ΔG_{CT}, and for the charge recombination process represented as ΔG_{CR}.

The reorganization energy comprises two parts, inner reorganization energy (λ_i) and external reorganization energy (λ_s)[70–72]. The λ_i originates due to a change in the equilibrium geometry of the donor (D) and acceptor (A) sites of the complex system during charge transfer processes and it includes contribution of hole and electron which is formulated as follows:

$$\lambda = \lambda_i + \lambda_s \tag{10}$$

$$\lambda_i = \lambda_h + \lambda_e \tag{11}$$

$$\lambda_h = E^+\left(D^0\right) - E^+\left(D^+\right) \tag{12}$$

$$\lambda_e = E^0\left(A^-\right) - E^0\left(A^0\right) \tag{13}$$

where $E^+(D^0)$ and $E^+(D^+)$ energies of radical cation donor at neutral geometry and optimal cation geometry. $E^0(A^-)$ and $E^0(A^0)$ are the energies of the neutral acceptor A at the anionic geometry and optimal ground state geometry, respectively. Calculating λ_s quantitatively is difficult as it involves electronic and nuclear polarizations. So, the value of λ_s is viewed as a constant equal to 0.3 eV.

The free energy change during charge recombination (ΔG_{CR}) can be calculated as given below Eq.[71–73]

$$\Delta G_{CR} = IP(D) - EA(A) \tag{14}$$

The IP(D) and EA(A) can be estimated as HOMO energy of donor and LUMO energy of acceptor, respectively. The free energy change at the CT process, ΔG_{CT}, can be estimated using the Rehm–Weller equation as follows[73].

$$\Delta G_{CT} = -\Delta G_{CR} - E_{S1}(D) \tag{15}$$

Where $E_{S1}(D)$ is the lowest excited-state energy of the free-base donor.

Data availability

The data that support the findings will be available from the authors if required.

Received: 23 June 2022; Accepted: 29 August 2022
Published online: 03 September 2022

References

1. Ball, M. *et al.* Conjugated macrocycles in organic electronics. *Acc. Chem. Res.* **52**, 1068–1078 (2019).
2. Zhang, S.-Q. *et al.* Donor–acceptor conjugated macrocycles: Synthesis and host–guest coassembly with fullerene toward photovoltaic application. *ACS Nano* **11**, 11701–11713 (2017).
3. Peng, X. *et al.* Selective adsorption of c60 in the supramolecular nanopatterns of donor–acceptor porphyrin derivatives. *Langmuir* **35**, 14511–14516 (2019).
4. Ito, H., Mitamura, Y., Segawa, Y. & Itami, K. Thiophene-based, radial π-conjugation: Synthesis, structure, and photophysical properties of cyclo-1,4-phenylene-2′,5′-thienylenes. *Angew. Chem.* **127**, 161–165 (2015).
5. Zhang, F., Götz, G., Winkler, H. D. F., Schalley, C. A. & Bäuerle, P. Giant cyclo[n]thiophenes with extended π conjugation. *Angew. Chem. Int. Ed.* **48**, 6632–6635 (2009).
6. Li, C. *et al.* A diketopyrrolopyrrole-based macrocyclic conjugated molecule for organic electronics. *J. Mater. Chem. C* **7**, 3802–3810 (2019).
7. Huang, Y., Kramer, E. J., Heeger, A. J. & Bazan, G. C. Bulk heterojunction solar cells: Morphology and performance relationships. *Chem. Rev.* **114**, 7006–7043 (2014).
8. dos Santos, J. M. *et al.* New thiophene-based conjugated macrocycles for optoelectronic applications. *J. Mater. Chem. C* **9**, 16257–16271 (2021).
9. Bandyopadhyay, A. & Pati, S. K. Role of donor–acceptor macrocycles in sequence specific peptide recognition and their optoelectronic properties: a detailed computational insight. *Phys. Chem. Chem. Phys.* **18**, 20682–20690 (2016).
10. Ball, M. *et al.* Macrocyclization in the design of organic n-type electronic materials. *J. Am. Chem. Soc.* **138**, 12861–12867 (2016).
11. Zhang, B. *et al.* Hollow organic capsules assemble into cellular semiconductors. *Nat. Commun.* **9**, 1957 (2018).
12. Ball, M. L. *et al.* Influence of molecular conformation on electron transport in giant, conjugated macrocycles. *J. Am. Chem. Soc.* **140**, 10135–10139 (2018).
13. Nakanishi, W. *et al.* [n]Cyclo-2,7-naphthylenes: synthesis and isolation of macrocyclic aromatic hydrocarbons having bipolar carrier transport ability. *Angew. Chem. Int. Ed.* **50**, 5323–5326 (2011).
14. Kayahara, E. *et al.* Gram-scale syntheses and conductivities of [10]cycloparaphenylene and its tetraalkoxy derivatives. *J. Am. Chem. Soc.* **139**, 18480–18483 (2017).
15. Peters, G. M. *et al.* Linear and radial conjugation in extended π-electron systems. *J. Am. Chem. Soc.* **142**, 2293–2300 (2020).
16. Xu, Y. *et al.* Highly strained, radially π-conjugated porphyrinylene nanohoops. *J. Am. Chem. Soc.* **141**, 18500–18507 (2019).
17. Ans, M., Ayub, K., Xiao, X. & Iqbal, J. Tuning opto-electronic properties of alkoxy-induced based electron acceptors in infrared region for high performance organic solar cells. *J. Mol. Liq.* **298**, 111963 (2020).
18. Ans, M., Ayub, K., Bhatti, I. & Iqbal, J. Designing indacenodithiophene based non-fullerene acceptors with a donor–acceptor combined bridge for organic solar cells. *RSC Adv.* **9**, 3605–3617 (2019).
19. Bai, H. *et al.* Acceptor–donor–acceptor small molecules based on indacenodithiophene for efficient organic solar cells. *ACS Appl. Mater. Interfaces* **6**, 8426–8433 (2014).
20. Ans, M., Iqbal, J., Bhatti, I. A. & Ayub, K. Designing dithienonaphthalene based acceptor materials with promising photovoltaic parameters for organic solar cells. *RSC Adv.* **9**, 34496–34505 (2019).
21. Yu, R. *et al.* Design and application of volatilizable solid additives in non-fullerene organic solar cells. *Nat. Commun.* **9**, 4645 (2018).
22. Shikita, S., Watanabe, G., Kanouchi, D., Saito, J. & Yasuda, T. Alternating donor–acceptor π-conjugated macrocycle exhibiting efficient thermally activated delayed fluorescence and spontaneous horizontal molecular orientation. *Adv. Photonics Res.* **2**, 2100021 (2021).
23. Lovell, T. C., Fosnacht, K. G., Colwell, C. E. & Jasti, R. Effect of curvature and placement of donor and acceptor units in cycloparaphenylenes: a computational study. *Chem. Sci.* **11**, 12029–12035 (2020).
24. Koçak, O., Duru, I. P. & Yavuz, I. Charge transfer and interface effects in co-assembled circular donor/acceptor complexes for organic photovoltaics. *Adv. Theory Simul.* **2**, 1800194 (2019).
25. Yuan, X. *et al.* Polythiophenes for organic solar cells with efficiency surpassing 17%. *Joule* **6**, 647–661 (2022).
26. Cobet, C. *et al.* Influence of molecular designs on polaronic and vibrational transitions in a conjugated push-pull copolymer. *Sci. Rep.* **6**, 35096 (2016).
27. Park, S., Lim, B. T., Kim, B., Son, H. J. & Chung, D. S. High mobility polymer based on a π-extended benzodithiophene and its application for fast switching transistor and high gain photoconductor. *Sci. Rep.* **4**, 5482 (2014).
28. da Silva, W. J., Schneider, F. K., Yusoff, M., Bin, A. R. & Jang, J. High performance polymer tandem solar cell. *Sci. Rep.* **5**, 18090 (2015).
29. Jung, I. H. *et al.* High thermoelectric power factor of a diketopyrrolopyrrole-based low bandgap polymer via finely tuned doping engineering. *Sci. Rep.* **7**, 44704 (2017).
30. Khalid, M. *et al.* Molecular engineering of indenoindene-3-ethylrodanine acceptors with A2–A1–D–A1–A2 architecture for promising fullerene-free organic solar cells. *Sci. Rep.* **11**, 20320 (2021).
31. Xue, Z.-X. *et al.* Non-fused molecular photovoltaic acceptor with a planar core structure enabled by bulky and embracing-type side chains. *J. Mater. Chem. C* **10**, 2945–2949 (2022).
32. Khursan, S. L. & Akhmetshina, E. S. Interplay of the ring and steric strains in the highly substituted cyclopropanes. *J. Phys. Chem. A* **125**, 7607–7615 (2021).
33. Colwell, C. E., Price, T. W., Stauch, T. & Jasti, R. Strain visualization for strained macrocycles. *Chem. Sci.* **11**, 3923–3930 (2020).
34. Bogdan, A. R., Jerome, S. V., Houk, K. N. & James, K. Strained cyclophane macrocycles: Impact of progressive ring size reduction on synthesis and structure. *J. Am. Chem. Soc.* **134**, 2127–2138 (2012).
35. Segawa, Y., Omachi, H. & Itami, K. Theoretical studies on the structures and strain energies of cycloparaphenylenes. *Org. Lett.* **12**, 2262–2265 (2010).
36. Wang, Y.-L., Li, Q.-S. & Li, Z.-S. End-capped group manipulation of fluorene-based small molecule acceptors for efficient organic solar cells. *Comput. Mater. Sci.* **156**, 252–259 (2019).
37. Ahmed, S. & Kalita, D. J. End-capped group manipulation of non-fullerene acceptors for efficient organic photovoltaic solar cells: A DFT study. *Phys. Chem. Chem. Phys.* **22**, 23586–23596 (2020).
38. Kuzmich, A., Padula, D., Ma, H. & Troisi, A. Trends in the electronic and geometric structure of non-fullerene based acceptors for organic solar cells. *Energy Environ. Sci.* **10**, 395–401 (2017).

39. Lv, Y. *et al.* Single cycloparaphenylene molecule devices: achieving large conductance modulation via tuning radial π-conjugation. *Sci. Adv.* **7**, eabk3095 (2021).
40. Oshi, R., Abdalla, S. & Springborg, M. The impact of functionalization of organic semiconductors by electron donating groups on the reorganization energy. *Eur. Phys. J. D* **73**, 124 (2019).
41. Ajmal, M. *et al.* Designing indaceno thiophene–based three new molecules containing non-fullerene acceptors as strong electron withdrawing groups with DFT approaches. *J. Mol. Model.* **25**, 311 (2019).
42. Sahu, H. & Panda, A. N. Computational investigation of charge injection and transport properties of a series of thiophene–pyrrole based oligo-azomethines. *Phys. Chem. Chem. Phys.* **16**, 8563 (2014).
43. Khalid, M. *et al.* Exploration of efficient electron acceptors for organic solar cells: rational design of indacenodithiophene based non-fullerene compounds. *Sci. Rep.* **11**, 19931 (2021).
44. Bhattacharya, L., Sharma, S. & Sahu, S. Enhancement of air stability and photovoltaic performance in organic solar cells by structural modulation of bis-amide-based donor-acceptor copolymers: A computational insight. *Int. J. Quantum Chem.* **121**, e26524 (2021).
45. Zhao, X. & Zhan, X. Electron transporting semiconducting polymers in organic electronics. *Chem. Soc. Rev.* **40**, 3728–3743 (2011).
46. Wang, Q. *et al.* Non-fullerene acceptor-based solar cells: from structural design to interface charge separation and charge transport. *Polymers* **9**, 692 (2017).
47. Bary, G. *et al.* Designing small organic non-fullerene acceptor molecules with diflorobenzene or quinoline core and dithiophene donor moiety through density functional theory. *Sci. Rep.* **11**, 19683 (2021).
48. Cancès, E., Mennucci, B. & Tomasi, J. A new integral equation formalism for the polarizable continuum model: Theoretical background and applications to isotropic and anisotropic dielectrics. *J. Chem. Phys.* **107**, 3032–3041 (1997).
49. Bednarz, M., Reineker, P., Mena-Osteritz, E. & Bäuerle, P. Optical absorption spectra of linear and cyclic thiophenes—selection rules manifestation. *J. Lumin.* **110**, 225–231 (2004).
50. Park, K. H., Kim, W., Yang, J. & Kim, D. Excited-state structural relaxation and exciton delocalization dynamics in linear and cyclic π-conjugated oligothiophenes. *Chem. Soc. Rev.* **47**, 4279–4294 (2018).
51. Han, G., Hu, T. & Yi, Y. Reducing the singlet–triplet energy gap by end-group π−π stacking toward high-efficiency organic photovoltaics. *Adv. Mater.* **32**, 2000975 (2020).
52. Qiu, W. & Zheng, S. Designing and screening high-performance non-fullerene acceptors: A theoretical exploration of modified Y6. *Sol. RRL* **5**, 2100023 (2021).
53. Salim, M., Rafiq, M., Khera, R. A., Arshad, M. & Iqbal, J. Amplifying the photovoltaic properties of azaBODIPY core based small molecules by terminal acceptors modification for high performance organic solar cells: A DFT approach. *Sol. Energy* **233**, 31–45 (2022).
54. Bhatta, R. S. & Tsige, M. Chain length and torsional dependence of exciton binding energies in P3HT and PTB7 conjugated polymers: A first-principles study. *Polymer* **55**, 2667–2672 (2014).
55. Lu, T. & Chen, F. Multiwfn: A multifunctional wavefunction analyzer. *J. Comput. Chem.* **33**, 580–592 (2012).
56. Martin, R. L. Natural transition orbitals. *J. Chem. Phys.* **118**, 4775–4777 (2003).
57. Frisch, M. J. *et al. Gaussian 16, Revision C.01* (Gaussian Inc., Wallingford, CT, 2016).
58. Wang, Q., Zeng, Z., Chen, X., Liu, Q. & Xu, M. Rational design non-fullerene acceptor-based high efficiency BHJ polymer solar cells through theoretical investigations. *J. Photochem. Photobiol. Chem.* **383**, 111985 (2019).
59. de Boer, R. W. I. *et al.* Space charge limited transport and time of flight measurements in tetracene single crystals: A comparative study. *J. Appl. Phys.* **95**, 1196–1202 (2004).
60. Ostroverkhova, O. Organic optoelectronic materials: mechanisms and applications. *Chem. Rev.* **116**, 13279–13412 (2016).
61. Wang, L., Li, T., Shen, Y. & Song, Y. A theoretical study of the electronic structure and charge transport properties of thieno[2,3-b] benzothiophene based derivatives. *Phys. Chem. Chem. Phys.* **18**, 8401–8411 (2016).
62. Ahmed, S. & Kalita, D. J. Charge transport in isoindigo-dithiophenepyrrole based D–A type oligomers: A DFT/TD-DFT study for the fabrication of fullerene-free organic solar cells. *J. Chem. Phys.* **149**, 234906 (2018).
63. Wang, L., Li, T., Shen, Y. & Song, Y. A theoretical study of the electronic structure and charge transport properties of thieno[2,3-b] benzothiophene based derivatives. *Phys. Chem. Chem. Phys.* **18**, 8401–8411 (2016).
64. Watanabe, K., Segawa, Y. & Itami, K. A theoretical study on the strain energy of helicene-containing carbon nanobelts. *Chem. Commun.* **56**, 15044–15047 (2020).
65. Marcus, R. A. Electron transfer reactions in chemistry: Theory and experiment. *Rev. Mod. Phys.* **65**, 599–610 (1993).
66. Zheng, Z., Tummala, N. R., Fu, Y.-T., Coropceanu, V. & Brédas, J.-L. Charge-transfer states in organic solar cells: Understanding the impact of polarization, delocalization, and disorder. *ACS Appl. Mater. Interfaces* **9**, 18095–18102 (2017).
67. Hsu, C.-P. The electronic couplings in electron transfer and excitation energy transfer. *Acc. Chem. Res.* **42**, 509–518 (2009).
68. Wang, L. *et al.* Computational methods for design of organic materials with high charge mobility. *Chem. Soc. Rev.* **39**, 423–434 (2010).
69. Ning, L., Han, G. & Yi, Y. Intra-chain and inter-chain synergistic effect gives rise to high electron mobilities for naphthalenediimide based copolymers. *J. Mater. Chem. C* **8**, 16527–16532 (2020).
70. Biswas, S., Pramanik, A., Pal, S. & Sarkar, P. A theoretical perspective on the photovoltaic performance of s, n-heteroacenes: An even–odd effect on the charge separation dynamics. *J. Phys. Chem. C* **121**, 2574–2587 (2017).
71. Liu, T. & Troisi, A. Absolute rate of charge separation and recombination in a molecular model of the P3HT/PCBM interface. *J. Phys. Chem. C* **115**, 2406–2415 (2011).
72. Li, Y., Feng, Y. & Sun, M. Photoinduced charge transport in a BHJ solar cell controlled by an external electric field. *Sci. Rep.* **5**, 13970 (2015).
73. Pandey, L. *Theoretical Studies of the Structure-Property Relationships of Hole- and Electron-Transport Materials for Organic Photovoltaic Applications* (2013).

Acknowledgements

S.H thanks DST-National Supercomputing Mission (NSM) for the research fellowship. M.K.R thank Department of Science and Technology (DST), New Delhi, India (DST/INSPIRE/04/2017/001393), for providing research fellowship under the DST-INSPIRE faculty scheme. M.K.R also thank Department of Science and Technology (DST), New Delhi, India for providing the access to supercomputers under DST- National Supercomputing Mission (NSM) (Ref No: DST/NSM/R&D_HPC_Applications/2021/16) project.

Author contributions

Conceptualization, M.K.R.; methodology, S.H. and M.K.R.; S.H. performed the calculations and initial data analysis; S.H. and M.K.R. contributed to discussion of the results; writing—original draft preparation, S.H.; Final version correction M.K.R.

Competing interests
The authors declare no competing interests.

Additional information
Supplementary Information The online version contains supplementary material available at https://doi.org/10.1038/s41598-022-19348-5.

Correspondence and requests for materials should be addressed to M.K.R.

Reprints and permissions information is available at www.nature.com/reprints.

Publisher's note Springer Nature remains neutral with regard to jurisdictional claims in published maps and institutional affiliations.